Electronic Spectra and Electronic Structures of $[Zr_6Cl_{12}Z]Cl_6^{n-}$ (Z = Be, B, Fe) Clusters

Marcus R. Bond and Timothy Hughbanks*

Department of Chemistry, Texas A&M University, College Station, Texas 77843-3255

Received May 4, 1992

Octahedral metal clusters of the type $M_6X_{18}^{n-}$ (X = halogen; n = 2–4) are well-known for M = Nb or Ta. More recently, a diverse zirconium-based cluster chemistry has emerged in which analogous zirconium clusters are stabilized by the encapsulation of a wide variety of interstitial elements. Despite extensive synthetic work and reports of several electronic structure calculations, no spectroscopic measurements of these have been reported. The electronic spectra of $Zr_6Cl_{18}Z^{n-}$ clusters (n = 2–6; Z = Be, B, Fe) have been recorded both in the solid state (by diffuse reflectance) and in acetonitrile solution. Main-group-centered clusters are typically dark orange or red to black, while transition-metal-centered clusters are typically green, blue, or purple. Main-group-centered clusters exhibit strong bands in the near-IR region (800–1200 nm), while transition-metal-centered clusters have, so far, exhibited their longest wavelength band in the visible region (~630 nm). Because of the chemical versatility that interstitial variation allows, spectral features that have otherwise been ambiguously assigned can now be assigned convincingly. In particular, unsettled aspects of the extensively studied niobium and tantalum systems become much clearer when comparison with the zirconium clusters is made. Extended Hückel calculations are shown to provide correct orbital energy orderings, though absolute transition energies are only in fair agreement with experiment.

Introduction

Among the oldest prototypes of inorganic cluster chemistry are the octahedral $[M_6X_{12}^{n+}]L_6$ (M = Nb, Ta; X = halide; n = 2–4; L = two-electron-donor ligand(s)).[1-3] Here the six metal atoms are arranged in an octahedral array with the twelve inner halides bridging every edge of the octahedron and the six ausser ligands capping every vertex. (Following common practice, we write $M_6X_{12}^{n+}$ to represent the $M_6X_{12}X_6^{n-}$ species unless the ausser ligands are known to differ elementally from the inner halides.) These clusters have received decades of scrutiny, during which investigators examined their chemical, structural, and spectroscopic properties. As one deduces from the formal charges that these clusters can bear, they are normally stable when the number of electrons available for cluster bonding is in the range from 14 to 16, at least as they are formed in high-temperature reactions in the solid state. In the past decade, Corbett and co-workers have developed a beautiful and extensive chemistry of analogous zirconium clusters where, in compensation for the fewer number of electrons that zirconium has to offer for cluster bonding, interstitial atoms are invariably encapsulated.[4-11] Despite the wealth of information we have concerning these clusters' proclivity for binding different interstitials and their structural versatility in intercluster binding, very little is known of their physical properties. In particular, theoretical treatments which rationalize these clusters' stability have little direct experimental support.[4-8,12,13]

Nature allows many isoelectronic extrapolations from the "empty" $[Nb_6Cl_{12}^{4+}]L_6$ cluster to interstitially stabilized clusters $[(Zr_6Z)Cl_{12}^{n+}]L_6$ (if Z = Be, n = 0; if Z = B, n = 1; if Z = C, n = 2; if Z = N, n = 3) (**1** and **2**, respectively). As examples,

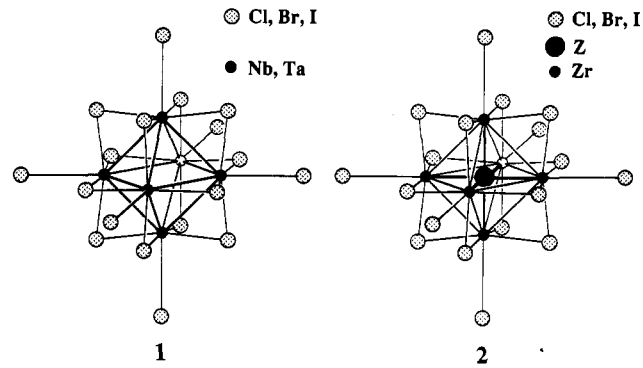

1 **2**

each of the cluster compounds $[(CH_3CH_2)_4N]_2Nb_6Cl_{18}$,[14] $Zr_6Cl_{15}N$, $KZr_6Cl_{15}C$, $Zr_6Br_{14}C$, $Zr_6Cl_{13}B$, $CsZr_6I_{14}B$, $RbZr_6Cl_{13}Be$, and $Zr_6Cl_{13}Be$[15,16] has 14 electrons available for cluster bonding, when one includes the interstitials' electrons in the counting scheme. Electron counts different from 14 are encountered in the zirconium system (e.g., $CsZr_6I_{14}C$, $Zr_6I_{12}B$, and $Zr_6Cl_{12}H$)[4,5,17] but are less common—especially among chlorides. However, when the interstitial element is a transition metal, the electron count of greatest stability shifts from 14 to 18.[8] Thus, the compounds $Zr_6I_{14}Fe$, $CsZr_6I_{14}Mn$, $Zr_6Cl_{15}Co$, $LiZr_6Cl_{15}Fe$, $Li_2Zr_6Cl_{15}Mn$, and $Cs_3(ZrCl_5)(Zr_6Cl_{15}Mn)$ have all been synthesized.[6,18,19] It should be noted that interstitial stabilization of clusters and condensed cluster compounds has proven to be a useful synthetic strategy in the metal-rich chemistry of the rare-earth-metal halides and early-transition-metal chalcogenides.

We have begun an investigation of the optical and magnetic properties of this class of clusters. Our observations will provide some more direct experimental tests of the theoretical bonding picture that one of us has helped to construct for the zirconium halide systems.[4-7] Both the symmetry and chemical versatility

* To whom correspondence should be addressed.

(1) Vaughan, P. A.; Sturtivant, J. H.; Pauling, L. *J. Am. Chem. Soc.* **1950**, *72*, 5477.
(2) Pauling, L. *The Nature of the Chemical Bond*, 3rd ed.; Cornell University Press: Ithaca, NY, 1960.
(3) Bauer, D.; Schnering, H. *Z. Anorg. Allg. Chem.* **1968**, *361*, 259.
(4) Smith, J. D.; Corbett, J. D. *J. Am. Chem. Soc.* **1985**, *107*, 5704.
(5) Smith, J. D.; Corbett, J. D. *J. Am. Chem. Soc.* **1986**, *108*, 1927.
(6) Hughbanks, T.; Corbett, J. D. *J. Am. Chem. Soc.* **1986**, *108*, 8289.
(7) Hughbanks, T.; Corbett, J. D. *J. Am. Chem. Soc.* **1988**, *110*, 1511.
(8) Hughbanks, T. *Prog. Solid State Chem.* **1989**, *19*, 329.
(9) Ziebarth, R. P.; Corbett, J. D. *J. Am. Chem. Soc.* **1988**, *110*, 1132.
(10) Ziebarth, R. P.; Corbett, J. D. *Acc. Chem. Res.* **1989**, *22*, 256.
(11) Ziebarth, R. P.; Corbett, J. D. *J. Am. Chem. Soc.* **1989**, *111*, 3272.
(12) Zhenyang, L.; Mingos, D. M. P. *J. Organomet. Chem.* **1988**, *339*, 367.
(13) Mingos, D. M. P.; Wales, D. J. *Introduction to Cluster Chemistry*; Prentice Hall: Englewood Cliffs, NJ, 1990.
(14) Mackay, R. A.; Schneider, R. F. *Inorg. Chem.* **1967**, *6*, 549.
(15) Ziebarth, R. P.; Corbett, J. D. *J. Am. Chem. Soc.* **1985**, *107*, 4571.
(16) Ziebarth, R. P.; Corbett, J. D. *J. Am. Chem. Soc.* **1987**, *109*, 4844.
(17) Ziebarth, R. P.; Corbett, J. D. *J. Solid State Chem.* **1989**, *80*, 56.
(18) Zhang, J.; Corbett, J. D. *Inorg. Chem.* **1991**, *30*, 431.
(19) Zhang, J.; Corbett, J. D. Private communication.

0020-1669/92/1331-5015$03.00/0

that this class of clusters exhibits are very useful "knobs" in our investigations, allowing for convincing assignments of spectral features that might otherwise prove ambiguous. In particular, we shall show that unsettled aspects of the extensively studied niobium and tantalum systems become much clearer when comparison with the zirconium clusters is made.

Experimental Procedures

Preparative Information. $Rb_5Zr_6Cl_{18}B$, $K_3Zr_6Cl_{15}Be$, and $KZr_6Cl_{15}Fe$ were synthesized by heating stoichiometric amounts of alkali-metal halide, zirconium powder, $ZrCl_4$, and amorphous boron, beryllium, or $FeCl_2$ in a sealed tantalum tube at 850 °C for 2 weeks.[9,11,20] All chlorides were sublimed under dynamic vacuum at least three times except for the alkali-metal and ammonium chlorides which were sublimed once. Zirconium powder was prepared from zirconium metal foil by a hydrogenation–dehydrogenation procedure previously described.[4] Amorphous boron (Aldrich) was used as received. Products were identified by their Guinier X-ray powder diffraction patterns.

Solid samples were dissolved in reagent grade acetonitrile which had refluxed over CaH_2 for several hours and then distilled under dry nitrogen or argon. Et_4NCl was dried at 100 °C under dynamic vacuum and added to the solutions of $KZr_6Cl_{15}Fe$ and $K_3Zr_6Cl_{15}Be$ in a 30:1 molar ratio with the intention of completely anating the dissolved cluster. Dissolution of $Rb_5Zr_6Cl_{18}B$ was aided by the addition of a 15-fold molar excess of 18-crown-6. Both the solid and solution forms of these compounds are extremely air sensitive, and appropriate techniques were employed in their preparation and handling.

Spectroscopic Measurements. Spectra were measured on a Cary 2300 spectrophotometer in both transmission and diffuse reflectance modes. Solution samples were contained in a 1 cm path length quartz cuvette fitted with a rubber septum to exclude air, except for the $KZr_6Cl_{15}Fe$ sample which was contained in a specially adapted, 1 mm path length quartz cuvette. Samples for diffuse reflectance were finely ground and deposited atop a layer of $BaSO_4$ in an aluminum sample holder. $BaSO_4$ was dried at 850 °C prior to use. A quartz plate was attached by a ring of silicone grease around the rim of the sample holder and served to hold the sample in place and to exclude air. Spectral baseline corrections were made relative to distilled acetonitrile (in transmission mode) and powdered $BaSO_4$ in diffuse reflectance mode. For the partially soluble $Rb_5Zr_6Cl_{18}B$ and $K_3Zr_6Cl_{15}Be$ cluster compounds, concentrations were determined through Mohr titration of chloride ion.[21] Concentrations of $KZr_6Cl_{15}Fe$ solutions were calculated after complete dissolution of a known mass of solid in a known volume of solvent.

Results

The prominent features of the diffuse reflectance spectrum of $Rb_5Zr_6Cl_{18}B$, shown in Figure 1a, are the two peaks in the near-infrared region: a broad, weak peak centered at 7700 cm^{-1} that merges into a narrower, stronger peak centered at 11 700 cm^{-1}. A broad, unresolved absorption is found above approximately 15 000 cm^{-1}. The spectrum of the cluster in solution, shown in Figure 1b, yields a low intensity peak at 11 400 cm^{-1} (in close correspondence with the position of the stronger peak in the reflectance spectrum) but also several peaks in the visible and UV regions which correspond in position to the unresolved absorption found in the reflectance data. This latter group of peaks contains a shoulder at 15 800 cm^{-1} (with about the same intensity as the 11 400-cm^{-1} peak) and distinct maxima at 21 800, 25 300 (the most intense), and 30 900 cm^{-1}. Several interfering solvent peaks in the 6000–9000-cm^{-1} region prevented detection of the lowest energy peak observed in the solid spectrum.

The solution spectrum of $K_3Zr_6Cl_{15}Be$ is similar to that of the boron-centered analog, but the higher reactivity of the beryllium-centered cluster in solution makes determination of the spectrum more difficult. Rogel and Corbett have shown that the 14-electron beryllium-centered cluster is easily oxidized in acetonitrile solution to a 12-electron analog.[20] They report a deep red color after initial solution of the 14-electron cluster and precipitation of black

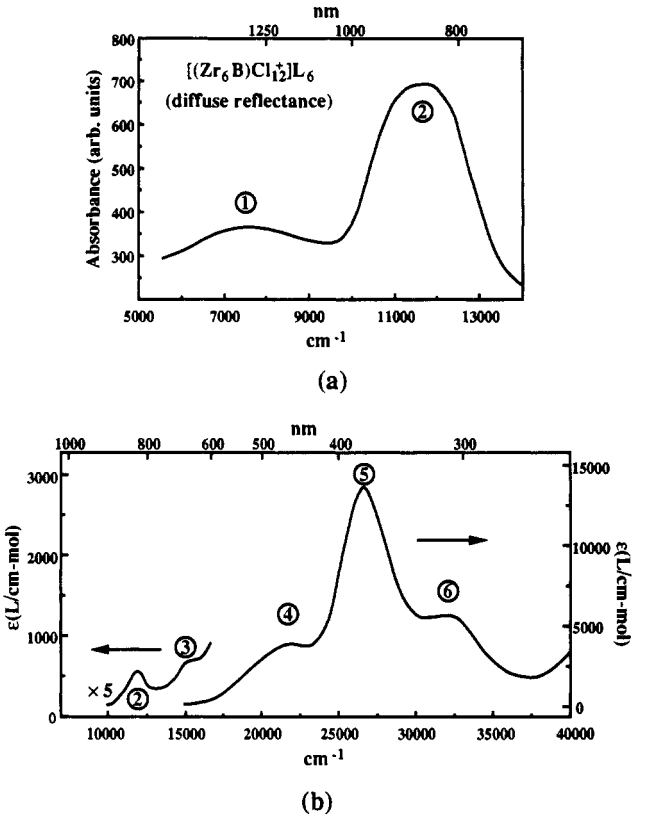

Figure 1. (a) Near-infrared diffuse reflectance spectrum of powdered $Rb_5Zr_6Cl_{18}B$. (b) Spectrum of $Rb_5Zr_6Cl_{18}B$ in acetonitrile.

crystals of the 12-electron species after cooling over a period of several weeks.[22] $K_3Zr_6Cl_{15}Be$ dissolves in acetonitrile to give a wine red solution which is stable for several hours and gives a spectrum (Figure 2a) that correlates to the near-IR reflectance spectrum of the solid. Upon purposeful introduction of air, the solution changes to an intense purple and eventually dark blue and exhibits the spectrum shown in Figure 2b. If air is not carefully excluded from the sample, the solution rapidly evolves from red to purple in color with the spectrum likewise evolving from that in Figure 2a to a weighted sum of spectra a and b in Figure 2. This bluish-purple solution is most likely that of the oxidized 12-electron cluster reported by Rogel and Corbett; however we have not yet been able to confirm this supposition.

Like that of the boron-centered cluster, the spectrum of the beryllium-centered cluster exhibits two weak peaks in the near-IR region, the less intense peak at 8300 cm^{-1} and the more intense peak at 10 900 cm^{-1}, with molar absorptivities comparable to those of the boride. The reflectance spectrum of the dark red solid clearly shows the presence of the latter peak (centered at 10 800 cm^{-1}) but shows the former only weakly. Two more intense peaks are found in the visible–UV region at 19 600 and 26 000 cm^{-1}, with the first peak the weaker of the two. The shoulder found at 15 800 cm^{-1} in the boride spectrum is not apparent in the beryllide spectrum, although it may be responsible for the asymmetry of the peak at 19 600 cm^{-1}, which has a long tail trailing to higher wavelength. The spectrum of the oxidized solution is similar to that of the unoxidized cluster but shows two important differences. First, the relative intensities of the two near-IR peaks reverse and the longer wavelength peak is blue-shifted from 8300 to 9100 cm^{-1}. Second, the relative intensities of the two peaks in the visible–UV region are also reversed and both are shifted to lower energy: 18 100 and 25 000 cm^{-1}.

The solid and solution spectra of $KZr_6Cl_{15}Fe$ are remarkable for the complete absence of measurable intensity in the near-IR region (see Figure 3). The lowest energy transitions are found

(20) Rogel, F.; Corbett, J. D. *J. Am. Chem. Soc.* **1990**, *112*, 8198.
(21) Swift, E. H. *Introductory Quantitative Analysis*; Prentice-Hall: New York, 1950.
(22) Rogel, F. Ph.D. Thesis, Iowa State University, 1991.

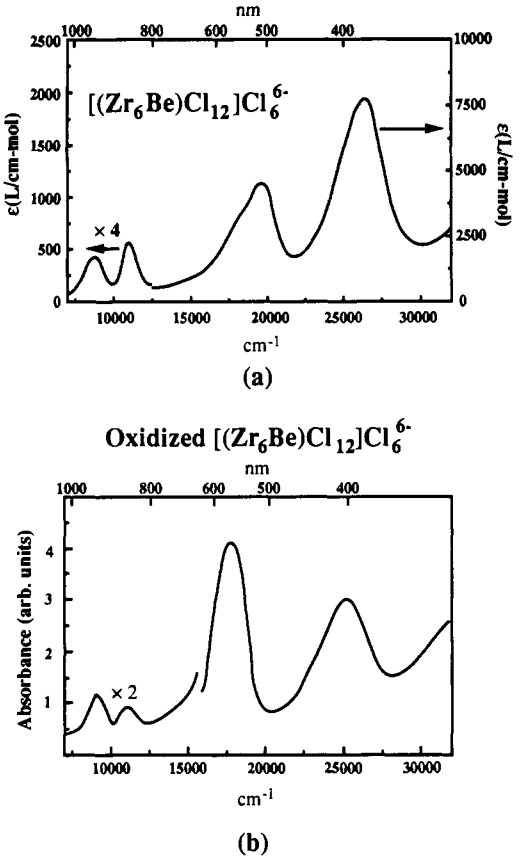

Figure 2. (a) Spectrum of $K_3Zr_6Cl_{15}Be$ in acetonitrile. (b) Spectrum of an acetonitrile solution of $K_3Zr_6Cl_{15}Be$ after oxidation by intentional exposure to air.

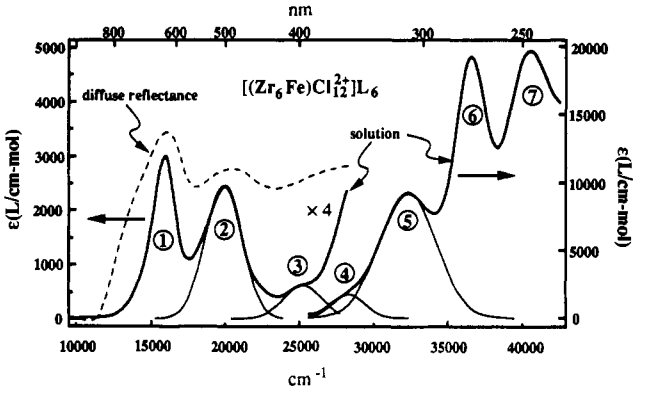

Figure 3. Spectrum of $KZr_6Cl_{15}Fe$. The dashed line is the diffuse reflectance spectrum; the solid line is an acetonitrile solution spectrum. Individual peaks are indicated by the localized Gaussian curves under the solution spectrum.

at 16 000 and 20 100 cm^{-1} in both the diffuse reflectance (dashed line in Figure 3) and solution (solid line in Figure 3) spectra. Molar absorptivities for these two peaks are at least 5 times greater than those of the lowest energy transitions in either main-group-centered cluster and probably arise from very different types of transitions (see below). These two peaks for the iron-centered cluster are followed by a weaker shoulder at 25 300 cm^{-1} and a series of intense absorptions at higher energy: a shoulder at 32 000 cm^{-1} with intensity comparable to that of the first two peaks, followed by three distinct maxima at 32 300, 36 500, and 40 300 cm^{-1}.

Similarity between diffuse reflectance and solution spectra confirm the presence of the $(Zr_6Z)Cl_{12}^{n+}$ cluster core in solution, as was previously established by Rogel and Corbett through crystallographic analysis of cluster compounds recrystallized from acetonitrile.[20] Some questions remain as to the exact nature of the ausser ligands in solution. However, all cluster species recrystallized from acetonitrile in the presence of excess chloride show the full complement of eighteen coordinated chlorides in spite of the presence of cocrystallized solvent. (For example, when $KZr_6Cl_{15}Fe$ is dissolved in acetonitrile with excess Et_4PCl, $(Et_4P)_4(Zr_6Cl_{18}Fe)\cdot 2CH_3CN$ is crystallized from solution.) It is thus apparent that cluster integrity is maintained upon dissolution. It is possible that the six ausser chlorides exchange with the solvent (the twelve inner chlorides being bound too tightly to react). If our measurements do not rule out this possibility, the similarity of solid and solution spectra indicate that such ligand displacement does not drastically alter the cluster spectra. In particular, the position of the pair of lowest energy peaks in the iron-centered cluster are virtually identical in both solid and solution. These results agree with those found for the analogous niobium and tantalum clusters, where only slight differences are observed between spectra in the solid and in any of a variety of solvents.[23,24]

Theoretical Framework

As a framework for discussing the electronic structure of these systems, it is useful to examine a molecular orbital diagram for $Nb_6Cl_{18}^{2-}$, calculated using the extended Hückel method and shown in Figure 4. Four bonding orbitals with a_{1g}, t_{1u}, t_{2g}, and a_{2u} symmetries in the O_h point group are identified by the calculation (listed in order of increasing energy) with the a_{1g}, t_{1u}, and t_{2g} levels filled in the 14-electron $Nb_6Cl_{18}^{2-}$ cluster. Since the calculation places the t_{2g} levels only slightly higher in energy than those of t_{1u} symmetry, the symmetry of the HOMO is computationally uncertain.

The cluster molecular orbitals are constructed as linear combinations of the metal 4d orbitals. If we consider a cube circumscribing the octahedral cluster and a metal atom centered at each face of the cube, then we can define local coordinate axes with the z-axis emanating radially from the cluster center for each atom and with the x- and y-axes in the plane of the face and parallel to the edges of the face. In this representation, the bridging (inner) halides are over the midpoints of the cube edges and the capping (ausser) halides are over the centers of the cube faces. The d-orbital contributions to the composition of each bonding orbital are as follows: The nondegenerate a_{1g} and a_{2u} molecular orbitals consist of atomic d_{z^2} and d_{xy} orbitals, respectively, uniformly distributed around the cluster, thus producing an MO with no angular nodes in $a_{1g}(d_{z^2})$ (**3**) but with three angular nodes (coinciding with the three equatorial planes of the octahedron) in $a_{2u}(d_{xy})$ (**4**). Molecular orbitals representative of

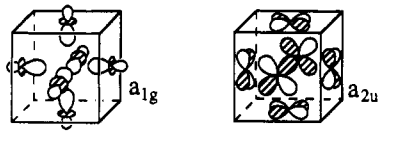

3 **4**

the two triply degenerate t_{1u} and t_{2g} levels can be constructed by placing d_{yz} or d_{xz} orbitals, respectively, about four equatorial positions and d_{z^2} and d_{xy} orbitals, respectively, in two axial positions such that there is a single angular node in the equatorial plane for t_{1u} (**5**) and two angular nodes (perpendicular to the equatorial plane) for t_{2g} (**6**). Note that orbital **6** consists of a bonding

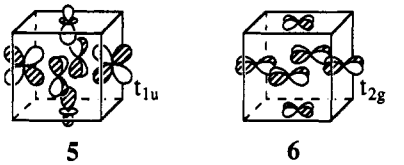

5 **6**

combination of $d_{xz,yz}$-type orbitals that mix in-phase with a combination of two d_{xy} orbitals. An out-of-phase mixing of the

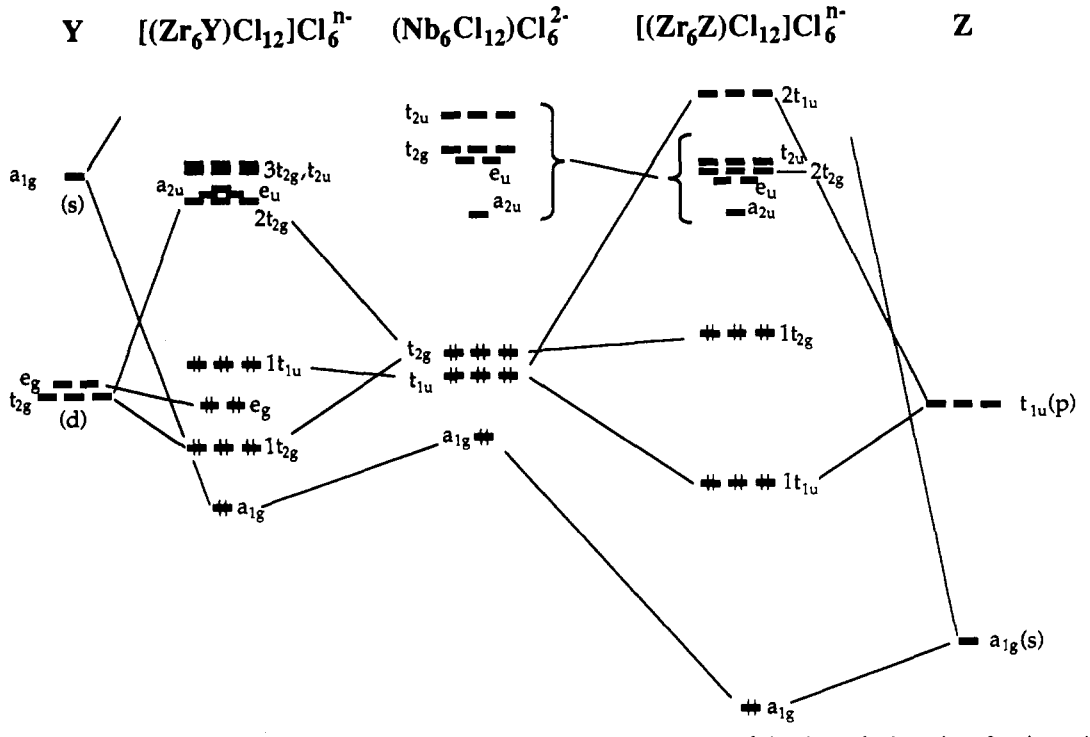

Figure 4. Schematic orbital interaction diagram showing the effect of the electronic structure of the cluster by insertion of an interstitial atom. The central orbital diagram belongs to the vacant $Nb_6Cl_{12}Cl_6^{2-}$ cluster, while the diagrams on far right and left show the valence orbitals for an isolated transition-metal (Y) or main-group (Z) atom. The valence orbitals of the interstitial interact with the valence orbitals of the vacant cluster to produce the unique orbital schemes for a transition-metal-centered cluster, $(Zr_6Y)Cl_{12}Cl_6^{n-}$ shown left of center, or a main-group cluster, $(Zr_6Z)Cl_{12}Cl_6^{n-}$, shown right of center.

two orbital sets gives rise to **7**, which is the lowest unoccupied level of t_{2g} symmetry shown in Figure 5 for $Nb_6Cl_{12}Cl_6^{2-}$.

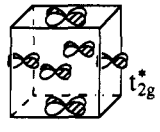

7

The evolution of these octahedral clusters' electronic structure when they are centered by interstitial atoms can be most easily understood by reference to the empty cluster's electronic structure and by allowing for two important effects. First, and most important, are the direct Zr–interstitial orbital interactions. A straightforward symmetry analysis of these interactions is usually sufficient to show how the presence of an interstitial perturbs the levels when compared with an empty cluster. Main-group interstitial a_{1g} and t_{1u} (2s and 2p) valence orbitals interact with Zr cage orbitals of like symmetry to form bonds with the surrounding Zr cluster atoms; for transition metals t_{2g}, e_g, a_{1g}, and t_{1u} (3d, 4s, and 4p) orbitals are available, the last of which is of less importance. Thus, attention can be focused on a few orbital symmetries in considering Zr–interstitial interactions. The second difference in cluster bonding arises from the expansion the Zr_6 cluster must undergo in order to accommodate interstitials. This has the general effect of reducing the strength of through-space Zr–Zr interactions and leads to a consequent narrowing in the spread of orbital energies for the hypothetical "empty" $[Zr_6Cl_{12}]L_6$ cluster. In the solid state, the octahedral symmetry of the cluster is often broken, though geometrical distortions are not so dramatic that an octahedral approximation of the electronic structure need be abandoned.

Considering the lowest energy manifold of empty orbitals in the 14-electron $Nb_6Cl_{18}^{2-}$ cluster (a_{2u}, e_u, t_{2g}, t_{1u} in order of increasing energy), there are a number of possible dipole-allowed transitions from the filled bonding levels: $1t_{2g} \rightarrow a_{2u}$, e_u, t_{2u} or $1t_{1u} \rightarrow 2t_{2g}$, labeled in Figure 4 as transitions 1–4 for the $Nb_6Cl_{12}Cl_6^{2-}$ system. In the corresponding interstitially-stabilized clusters, the valence orbitals of the interstitial atom interact strongly only with the Zr cage orbitals of the correct symmetry. Thus, while the spectra for the interstitially-stabilized clusters will bear some resemblance to that of the vacant Nb or Ta cluster, transitions originating from orbitals with interstitial mixing will be markedly changed if not altogether absent.

A factor that we will not address in the present paper, but which should be borne in mind when spectra using 1-electron-derived theories are interpreted, is the influence of electron correlation. It seems likely that the biggest influence of correlation effects in the present context will come from configurational mixing in closely spaced excited states. As an example for the $[Nb_6Cl_{12}^{4+}]L_6$ and $[(Zr_6B)Cl_{12}^{+}]L_6$ clusters, we will speak loosely of transitions between the t_{2g} HOMO and the two lowest lying unoccupied orbitals of a_{2u} and e_u symmetries. In each case, the electric-dipole-allowed transitions are between a ground state of A_{1g} symmetry and excited states of T_{1u} symmetry. It should be understood that the two excited T_{1u} states may involve significant configurational mixing, particularly because the two excited orbitals are close in energy and have appreciable overlap densities. These reservations notwithstanding, we will see that a convincing empirical case can be made for the use of 1-electron orbital assignments as indicative of the general nature of the transitions observed.

Group V Clusters: Previous Spectral Studies of $[M_6Cl_{12}^{n+}]L_6$ Compounds

An extensive body of work on the electronic spectra of $(Nb,Ta)_6Cl_{12}^{n+}$ (n = 2–4) has been published. Spreckelmeyer tabulated the spectral data acquired prior to 1969 and found good agreement between spectra taken by different workers and under different conditions.[23] In their definitive work, Fleming and McCarley carefully examined the solid and solution spectra for the

(23) Spreckelmeyer, V. B. *Z. Anorg. Allg. Chem.* **1969**, *365*, 225–242.
(24) Fleming, P. B.; McCarley, R. E. *Inorg. Chem.* **1970**, *9*, 1347.

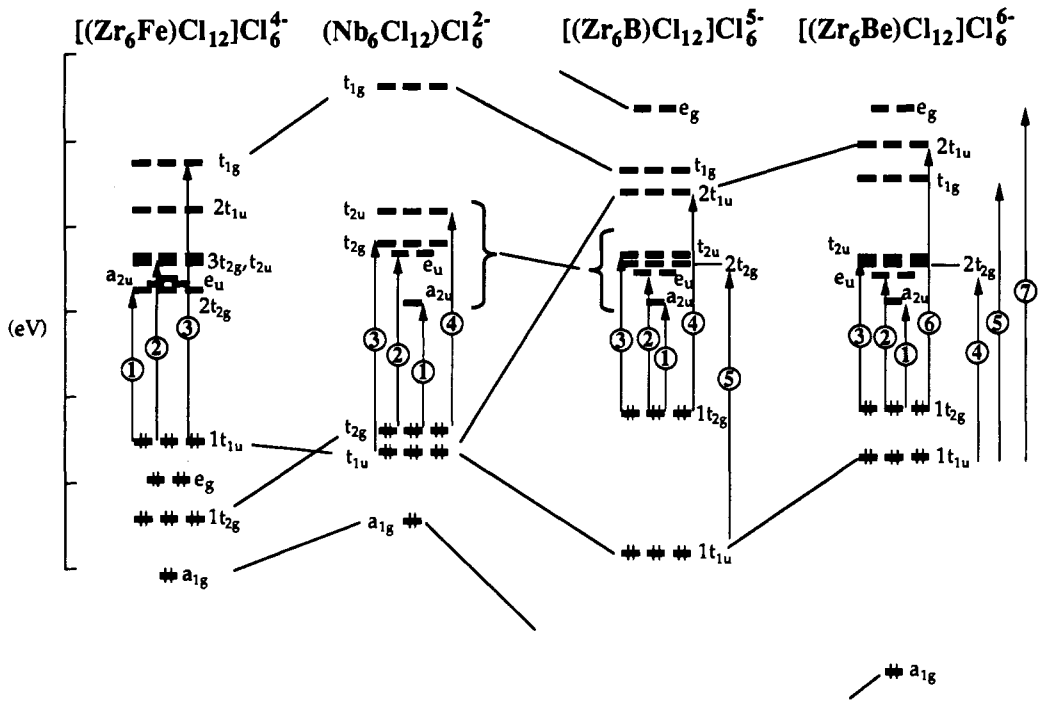

Figure 5. Energy diagram for the vacant $Nb_6Cl_{12}Cl_6^{2-}$ cluster (left of center) and the three interstitially stabilized clusters studied in this paper: $[(Zr_6Fe)Cl_{12}]Cl_6^{4-}$ (far left), $[(Zr_6B)Cl_{12}]Cl_6^{5-}$ (right of center), and $[(Zr_6Be)Cl_{12}]Cl_6^{6-}$ (far right). Absolute energies of the levels have been arbitrarily shifted to bring them onto the same level for purposes of comparison. Dipole-allowed transitions are denoted by the vertical arrows and are numbered in order of increasing transition energy. These numbers are correlated to the peak numbers of the spectra in Figures 1–3.

$(Nb,Ta)_6Cl_{12}^{n+}$ clusters in all oxidation states (n = 2–4) and the solution spectra for the $(Nb_6Cl_{12})Br_6^{2-}$ and $(Nb_6Br_{12})Br_6^{2-}$ clusters.[24] The strong similarity between their solid and solution spectra confirmed earlier conclusions, based on spectroscopic and conductivity measurements, that the Nb_6Cl_{12} cluster core is retained in solution. Comparison of the $(Nb_6Cl_{12})Cl_6^{2-}$ spectrum with those of $(Nb_6Cl_{12})Br_6^{2-}$ and $(Nb_6Br_{12})Br_6^{2-}$ reveals only slight changes in peak positions when the ausser chloride ions are replaced with bromide but large changes for those peaks above 29 000 cm^{-1} when all chlorides are replaced. The high-energy (>29 000 cm^{-1}) peaks were thus assigned to charge-transfer transitions originating from the inner halides, while it was concluded that the lower energy peaks arise from transitions between metal-based cluster orbitals. While we have not examined any halide variations, we certainly expect Cl → M charge-transfer transitions for Zr-based clusters to be at higher energy than those for Nb-based clusters. We are probably safe in assuming that no charge-transfer transitions will occur below 30 000 cm^{-1}.

Despite the abundance of experimental data collected over decades, there is surprisingly little consensus on their interpretation. This is primarily because of conflicting ideas about the symmetry and ordering of the cluster orbitals. An early molecular orbital calculation by Cotton and Haas posited four occupied cluster bonding orbitals with symmetries a_{1g}, t_{2g}, t_{1u}, and a_{2u} but with a somewhat uncertain order.[25] Robin and Kuebler proposed, on the basis of molecular orbital calculations and observed spectra, that electronic transitions for the 16-electron cluster originated instead from an $e_u^4t_{1u}^6t_{2g}^6$ ground configuration, although this clearly contradicts experimental evidence of a nondegenerate HOMO (see below).[26] Mackay and Schneider used an orbital scheme similar to that of Cotton and Haas, with the highest energy bonding orbital of a_{2u} symmetry, but their assignments were marred by the presence of a spurious peak in the spectrum.[14] Fleming and McCarley accepted this same orbital scheme but, on the basis of qualitative ligand field arguments, concluded that a_{1g} is the highest energy bonding orbital and made their assignments accordingly.[24] The magnetic circular dichroism (MCD) measurements later made by Robbins and Thomson should, in principle, be helpful in determining the correct spectral assignments, but their data are interpreted with a crystal field model that gives an inadequate account of the metal–metal bonding in the cluster.[27] They concluded that the occupied levels were of a_{1g}, t_{1u}, t_{1u}, and a_{2u} symmetries; to our knowledge, no attempt has been made to reinterpret the MCD data within a more conventional framework. More recent theoretical treatments present a mutually consistent picture that agrees qualitatively with that originally set forth by Cotton and Haas (see above).[28-30] Experimental interest in the spectroscopic properties of this class of compounds, however, has been dormant, so the current theory has not yet been tested against the experimental data and the spectral assignments remain uncertain.

One aspect of the electronic structure of Nb and Ta cluster systems about which there seems little doubt is the nature of the eighth metal-localized molecular orbital (i.e., the LUMO for the 14-electron clusters). Both the 14- and 16-electron systems are diamagnetic, indicating that the final 2 electrons occupy a nondegenerate orbital. The impressive Nb hyperfine splitting of the EPR line in the 15-electron $[Nb_6Cl_{12}^{3+}]Cl_6$ species proves the symmetrical distribution of spin density over all six Nb centers and the nondegenerate nature of a singly occupied orbital.[14,31] Measured isotropic g values near 2.0 for all 15-electron species,[32] including Nb_6F_{15} in the solid state,[33] indicates the universality of this electronic feature.

Spectra of Boron- and Iron-Centered Zirconium Clusters

Peak energies for the $(Zr_6B)Cl_{12}^+$, $(Zr_6Be)Cl_{12}$, and $(Zr_6Fe)Cl_{12}^{2+}$ clusters are compiled in Table I together with our transition

(25) Cotton, F. A.; Haas, T. E. *Inorg. Chem.* **1964**, *3*, 10.
(26) Robin, M. B.; Kuebler, N. A. *Inorg. Chem.* **1965**, *4*, 978.
(27) Robbins, D. J.; Thomson, A. J. *J. Chem. Soc., Dalton Trans.* **1972**, 2350.
(28) Wooley, R. G. *Inorg. Chem.* **1985**, *24*, 3519.
(29) Bursten, B. E.; Cotton, F. A.; Stanley, G. G. *Isr. J. Chem.* **1980**, *19*, 132.
(30) Burdett, J. K.; Hughbanks, T. *J. Am. Chem. Soc.* **1984**, *106*, 3101.
(31) Klendworth, D. D.; Walton, R. A. *Inorg. Chem.* **1981**, *20*, 1151.
(32) Converse, J. G.; McCarley, R. E. *Inorg. Chem.* **1970**, *9*, 1361.
(33) Bond, M.; Hughbanks, T. Unpublished research.

Table I. Assignments and Observed and Calculated Energies for Electronic Transitions of $Rb_5Zr_6Cl_{18}B$, $K_3Zr_6Cl_{15}Be$, and $KZr_6Cl_{15}Fe$ in Acetonitrile Solution

peak	transition	energy (10^3 cm^{-1}) obsd	calcd
	$(Zr_6B)Cl_{12}^{+}$ in CH_3CN		
1	$1t_{2g} \rightarrow a_{2u}$	7.3	10.5
2	$1t_{2g} \rightarrow e_u$	11.3	13.2
3	$1t_{2g} \rightarrow t_{2u}$	15.8	15.0
4	$1t_{2g} \rightarrow 2t_{1u}$	21.8	20.8
5	$1t_{1u} \rightarrow 2t_{2g}$	25.3	27.1
	$(Zr_6Be)Cl_{12}$ in CH_3CN		
1	$1t_{2g} \rightarrow a_{2u}$	8.3	10.6
2	$1t_{2g} \rightarrow e_u$	10.9	12.5
3	$1t_{2g} \rightarrow t_{2u}$	unobsd	13.4
4	$1t_{1u} \rightarrow 2t_{2g}$	19.6	18.1
5	$1t_{2g} \rightarrow 2t_{1u}$	26.0	26.4
	$(Zr_6Fe)Cl_{12}^{2+}$ in CH_3CN		
1	$1t_{1u} \rightarrow 2t_{2g}$	16.0	14.4
2	$1t_{1u} \rightarrow 3t_{2g}$	20.1	17.1
3	$1t_{1u} \rightarrow t_{1g}$	25.3	26.3
4	?	28.1	
5	?	32.1	
6	?	36.5	
7	?	40.3	

assignments and their energies as calculated by the extended Hückel method. A quick glance at the table reveals satisfactory agreement between the theoretical and experimental values, which is perhaps the best one can expect from an approximate model. The reasoning behind these spectral assignments and their implications for the electronic structure of these compounds are discussed below.

We begin by comparing the electronic spectra for the interstitially stabilized $[(Zr_6B)Cl_{12}]Cl_6^{5-}$, $[(Zr_6Be)Cl_{12}]Cl_6^{5-}$, and $[(Zr_6Fe)Cl_{12}]Cl_6^{4-}$ clusters with spectral data for the vacant $[Nb_6Cl_{12}]Cl_6^{2-}$ cluster. The close correspondence between the electronic spectra of the $[Nb_6Cl_{12}]Cl_6^{2-}$ and $[(Zr_6B)Cl_{12}]Cl_6^{5-}$ clusters in the near-IR region is very useful for interpretation. From the orbital ordering given by the extended Hückel calculations and electric dipole selection rules, we expect that the two peaks for $[Nb_6Cl_{12}]Cl_6^{2-}$ in the near-IR region are both transitions from the A_{1g} ground state to excited T_{1u} states, the first involving a 1-electron transition from the HOMO to the LUMO ($t_{2g} \rightarrow a_{2u}$) and the second involving a transition from the t_{2g} HOMO to next-to-lowest unoccupied e_u orbital. Because the symmetry of the valence orbitals of a main-group interstitial (Z) does not include any of these irreducible representations, two peaks are also expected in the near-IR region for all of the $(Zr_6Z)Cl_{12}^{n+}$ clusters. This is just what we observe; Figure 1 shows peaks centered at 7700 and 11 700 cm^{-1} in the diffuse reflectance near-IR spectrum of $Rb_5[(Zr_6B)Cl_{18}]$, the latter peak at the long wavelength end of the solution spectrum of the $[(Zr_6B)Cl_{12}]Cl_6^{5-}$ cluster shown in Figure 1b. Both near-IR peaks, however, are clearly visible in the solution spectrum of the beryllide analog (Figure 2a). The calculated transition energies in both compounds (10 500 and 13 200 cm^{-1} for the boride; 10 600 and 12 500 cm^{-1} for the beryllide) are higher than the experimental values but nonetheless predict a pair of peaks in the near-IR region.

The behavior of the iron-centered cluster, $[(Zr_6Fe)Cl_{12}]Cl_6^{4-}$, is relevant to support of our assignments for the $[Nb_6Cl_{12}^{4+}]L_6$ cluster and the main-group-centered zirconium analogs. Royal blue solutions of this cluster show no absorption at wavelengths longer than ~700 nm, leading us to conclude that the character of the HOMO and/or the LUMO is markedly different in the iron-centered cluster from that in the vacant or main-group-centered clusters. But, because neither of the low-lying unoccupied a_{2u} and e_u symmetry orbitals for the vacant cluster is of the appropriate symmetry to mix with any Fe valence orbitals, the relative energy shift for these levels (compared with those for $[(Zr_6B)Cl_{12}]Cl_6^{5-}$ clusters) will be primarily due to variations in the clusters' Zr–Zr distances. Such shifts should be modest because the a_{2u} and e_u orbitals, respectively, have only weak Zr–Zr bonding and antibonding characters. On the contrary, the vacant cluster's t_{2g} HOMO can effectively mix through direct Zr–Fe π bonding with the central iron d orbitals, and the very short Zr–Fe distances of 2.42 Å suggest that this π bonding is strong.

We conclude that the two lowest transitions for both $[(Zr_6B)Cl_{12}]Cl_6^{5-}$ and $[Nb_6Cl_{12}]Cl_6^{2-}$ are of the same character, involving the same HOMO and the same low-lying unoccupied levels. Assuming this to be the case, we can make significant progress in unraveling the frontier orbitals for both systems. A HOMO of t_{2g} symmetry is clearly indicated for the $[(Zr_6Z)Cl_{12}^{n+}]L_6$ clusters (Z = main-group element) and is probably the HOMO for $[Nb_6Cl_{12}^{4+}]L_6$ clusters as well. This latter assignment is not quite as certain, given the fact that transitions from the occupied t_{1u} orbital to the low-lying unoccupied a_{2u} and e_u orbitals are forbidden. The absence of any near-IR absorption in the $[(Zr_6Fe)Cl_{12}^{2+}]L_6$ system is strong support for the $1t_{2g} \rightarrow a_{2u}$ and $1t_{2g} \rightarrow e_u$ orbital assignments for the near-IR peaks for both the $[Nb_6Cl_{12}^{4+}]L_6$ system and the $[(Zr_6B)Cl_{12}^{+}]L_6$ systems.

The confidence with which we can make spectral assignments beyond this point varies with the system being considered and with uncertainties in the admittedly limited extended-Hückel-based interpretative theory. Still, the interstitially stabilized clusters are more easily handled because the number of energetically accessible, occupied orbitals is smaller.

For the $[(Zr_6B)Cl_{12}]_6^{5-}$ cluster, the t_{2g} HOMO must certainly be separated by an appreciable gap from the next-highest occupied t_{1u} level (we calculate 1.62 eV), since the latter orbital is stabilized by significant Zr–B bonding. Because $1t_{1u} \rightarrow a_{2u}$, e_u transitions are forbidden, we can conclude that the lowest energy transitions involving excitations from the t_{1u} level are likely to be found at energies $\gtrsim$3.0 eV. We then assign the peaks centered at 15 800 cm^{-1} as orbital excitation $1t_{2g} \rightarrow t_{2u}$ and the peaks at 21 800 and 25 300 cm^{-1}, respectively, as $1t_{2g} \rightarrow 2t_{1u}$ and $1t_{1u} \rightarrow 2t_{2g}$. Calculated values of 15 000, 20 800, and 27 100 cm^{-1} for these transitions agree reasonably well with the observed values.

The bonding t_{1u} orbital is not stabilized as much in the beryllium-centered cluster as in the boron analog because of the higher energy of the beryllium 2p orbitals. We therefore expect some differences in the visible and UV range of the spectrum reflecting allowed transitions arising from this level in addition to those arising from the t_{2g} HOMO. In fact, the $1t_{1u}$ level is now high enough in energy that we assign the peak at 19 600 cm^{-1} to a $1t_{1u} \rightarrow 2t_{2g}$ transition (calculated value: 18 100 cm^{-1}) and the peak at 26 000 cm^{-1} as $1t_{1u} \rightarrow t_{1g}$ or $1t_{2g} \rightarrow 2t_{1u}$, calculated values falling within 1500 cm^{-1} of one another by our calculation (24 900 and 26 400 cm^{-1}, respectively).

Two peaks at 15 960 and 20 050 cm^{-1} are conspicuous in the visible spectrum of the $[(Zr_6Fe)Cl_{12}]Cl_6^{4-}$ cluster. With a good degree of confidence, we assign these transitions to the respective orbital excitations $1t_{1u} \rightarrow 2t_{2g}$ and $1t_{1u} \rightarrow 3t_{2g}$. That the $1t_{1u}$ orbital is the HOMO seems to be an inescapable conclusion. As we have discussed above, the occupied $1t_{2g}$ orbital is strongly stabilized by Zr–Fe π bonding—in fact, we calculate this orbital to have 55.0% Fe character. Both the $2t_{2g}$ and $3t_{2g}$ levels carry some Fe–Zr antibonding character. The three t_{2g} levels shown for $(Zr_6Fe)Cl_{12}^{2+}$ arise from mixing between the Fe d(t_{2g}) orbitals with the two "empty cluster" combinations, **6** and **7**. The shoulder observed in the $[(Zr_6Fe)Cl_{12}]Cl_6^{4-}$ spectrum at approximately 25 270 cm^{-1} might be assigned to either a $e_g \rightarrow t_{2u}$ or a $1t_{1u} \rightarrow t_{1g}$ excitation. Assuming this assignment to be correct, the comparison between calculated orbital energy differences (14 400, 17 100, and 26 300 cm^{-1}) and the observed position of the first three peaks (15 960, 20 050, 25 270 cm^{-1}) is as good as one should expect from extended Hückel theory. Peak assignments at higher

energy are more difficult to make, since transitions from the bonding $1t_{2g}$ level are expected in addition to those from $1e_g$ and $1t_{1u}$. Unambiguous interpretation of this region of the spectrum awaits future work.

We think it is likely that the calculated relative positions of the $1t_{2g}$ and e_g Fe-localized orbitals are too high in energy. The relative position of these levels is quite sensitive to one of the most uncertain aspects of the extended Hückel parametrization: the relative energetic disposition of the Zr(4d) and Fe(3d) orbitals (the VSIE's—H_{ii}'s). Our parameters are used as they emerge from a charge-iterative calculation on a $(Zr_6Fe)I_{14}$ solid, as previously reported.[6] Such charge-iterative calculations are an attempt to account for the rather large and physically unrealistic charge densities that can accumulate on transition-metal atoms in extended Hückel calculations.[34] Such calculations are performed because there is otherwise no explicit way to account for differences in intraatomic e–e repulsion for metals in very different environments. Previous experience indicates that such calculations tend to overcompensate in adjusting VSIE's to reduce atomic charges. In the present context this means that while the Fe(3d) valence state ionization energy is lower than that for Zr(4d), the gap in the parameters is probably too small. On the other hand, recently reported extended Hückel calculations on $Th_6Br_{15}Fe$ use parameters with very large Fe(3d)–Th(6d) orbital energy differences and highly negative Fe charges are the result.[35,36] A self-consistent density functional calculation on these materials would probably yield better results in this regard.

Concluding Remarks

We believe that we have laid a useful foundation for the spectroscopic study of these systems, but there remains much quantitative work to be done and much information to be gained from the study of the spectroscopy of $[(Zr_6Z)X_{12}]^{n+}$ clusters. The study of chemical trends is always very revealing and the breadth of this class of compounds is now wide enough to be successfully exploited.

Energies for the dipole-allowed transitions from the extended Hückel calculation give satisfactory agreement with the observed values, as summarized in Table I. While these results are encouraging, further study is necessary to confirm our assignments. Systematic variation of the spectral data through a homologous series of compounds will aid in identifying the higher energy transitions, although it may ultimately be necessary to use more sophisticated techniques, such as MCD, to fully unravel the spectral assignments at higher energy. As it stands, the combination of theoretical calculations and spectral differences between main-group- and transition-metal-centered clusters has allowed a convincing assignment of the low-energy peaks as dipole-allowed transitions originating from a $1t_{2g}$ or $1t_{1u}$ HOMO, respectively. Since near-IR spectra of the main-group-centered Zr clusters and the vacant Nb clusters are quite similar, we can extend this conclusion to this latter cluster class as well. This new insight does resolve previous speculation that these weak near-IR features may actually arise from dipole-forbidden transitions from a_{1g} or $1t_{1u}$.[24,29]

Finally, our results show the sensitivity of the cluster spectra not only to the type of interstitial but also to the oxidation state of the cluster, as for the Be-centered system. This is not unexpected, since this result has been observed in the $(Nb,Ta)_6Cl_{12}^{n+}$ system as well, with the near-IR region acting as the most sensitive indicator of oxidation state.[24]

Acknowledgment. Partial support of this research was derived from a grant (010366-111) from the Exxon Education Foundation. We also acknowledge the National Science Foundation for its support through a Presidential Young Investigator Award (Grant DMR-8858151) and the Robert A. Welch Foundation for its support through Grant A-1132.

Appendix

Extended Hückel parameters appear in Table II. Structural parameters for $[(Zr_6Fe)Cl_{12}]Cl_3$ were taken from crystallographic data[18] and for $[(Zr_6B)Cl_{12}]Cl_6^{5-}$ from data for $Rb_5[(Zr_6B)Cl_{18}]$.[9,20] Orbital parameters for Fe and Zr were derived from a previously discussed charge-iterative EH-band calculation on a modestly idealized $(Zr_6Fe)I_{14}$ crystal.[6] Nb parameters were taken from previous work;[30] other parameters are standard.[37,38]

Table II. Parameters for EH Calculations

	orbital	H_{ii}, eV	ζ_1[a]	ζ_2[a]	c_1[b]	c_2[b]
Fe	3d	−9.35	5.55	1.80	0.5366	0.6678
	4s	−7.74	1.90			
	4p	−5.37	1.90			
Zr	4d	−8.59	3.84	1.505	0.6213	0.5798
	5s	−8.44	1.82			
	5p	−4.75	1.78			
Nb	4d	−12.10	4.08	1.64	0.6404	0.5313
	5s	−10.10	1.74			
	5p	−6.86	1.70			
Cl	3s	−30.0	2.36			
	3p	−15.0	2.04			
C	2s	−21.4	1.625			
	2p	−11.4	1.625			
B	2s	−15.2	1.30			
	2p	−8.5	1.30			

[a] Slater-type orbital exponents. [b] Coefficients used in double-ζ expansion.

(34) Ballhausen, C. J.; Gray, H. B. *Molecular Orbital Theory*; W. A. *Benjamin*, Inc.: New York, 1965.
(35) Decastro, L. F. P.; Muller, H. *J. Less-Common Met.* **1990**, *162*, 87–97.
(36) Böttcher, F.; Simon, A.; Kremer, R.; Buchkremer-Hermanns, H.; Cockroft, J. *Z. Anorg. Allg. Chem.* **1991**, *598/599*, 25.
(37) Whangbo, M.-H.; Evain, M.; Hughbanks, T.; Kertesz, M.; Wijeyesekera, S.; Wilker, C.; Zheng, C.; Hoffmann, R. *QCPE* **1989**, *9*, 61.
(38) Hoffmann, R. *J. Chem. Phys.* **1963**, *39*, 1397.